AFRL-RY-WP-TP-2019-0276

ANGLE- AND POLARIZATION-INDEPENDENT MID-INFRARED NARROWBAND OPTICAL FILTERS USING DENSE ARRAYS OF RESONANT CAVITIES (Preprint)

Shivashankar Vangala, Joshua R. Hendrickson, and Justin W. Cleary
EO/IR Components Branch
Aerospace Components Division

Ivan Avrutsky
Wayne State University

Evan M. Smith and Ricky Gibson
KBRWyle Laboratories

JANUARY 2020
Final Report

AIR FORCE RESEARCH LABORATORY
SENSORS DIRECTORATE
WRIGHT-PATTERSON AIR FORCE BASE, OH 45433-7320
AIR FORCE MATERIEL COMMAND
UNITED STATES AIR FORCE

REPORT DOCUMENTATION PAGE

Form Approved
OMB No. 0704-0188

1. REPORT DATE *(DD-MM-YY)*	2. REPORT TYPE	3. DATES COVERED *(From - To)*
January 2020	Journal Article Preprint	4 October 2019 –4 October 2019

4. TITLE AND SUBTITLE

ANGLE- AND POLARIZATION-INDEPENDENT MID-INFRARED NARROWBAND OPTICAL FILTERS USING DENSE ARRAYS OF RESONANT CAVITIES (Preprint)

5a. CONTRACT NUMBER
FA9550-19RYCOR048

5b. GRANT NUMBER

5c. PROGRAM ELEMENT NUMBER
N/A

6. AUTHOR(S)

Shivashankar Vangala, Joshua R. Hendrickson, and Justin W. Cleary (AFRL/RYDH)
Ivan Avrutsky (Wayne State University)
Evan M. Smith and Ricky Gibson (KBRWyle Laboratories)

5d. PROJECT NUMBER
N/A

5e. TASK NUMBER
N/A

5f. WORK UNIT NUMBER
N/A

7. PERFORMING ORGANIZATION NAME(S) AND ADDRESS(ES)

Air Force Research Laboratory
Sensors Directorate (AFRL/RYDH)
Wright-Patterson Air Force Base, OH 45433-7320
Air Force Materiel Command
United States Air Force

Wayne State University

KBRWyle Laboratories

8. PERFORMING ORGANIZATION REPORT NUMBER

9. SPONSORING/MONITORING AGENCY NAME(S) AND ADDRESS(ES)

Air Force Research Laboratory
Sensors Directorate
Wright-Patterson Air Force Base, OH 45433-7320
Air Force Materiel Command
United States Air Force

Air Force Office of Scientific Research Public Affairs (AFOSR)
875 North Randolph Street, Suite 325, Room 3112
Arlington, VA 22203

10. SPONSORING/MONITORING AGENCY ACRONYM(S)
AFRL/RYDH

11. SPONSORING/MONITORING AGENCY REPORT NUMBER(S)
AFRL-RY-WP-TP-2019-0276

12. DISTRIBUTION/AVAILABILITY STATEMENT
Approved for public release; distribution is unlimited.

13. SUPPLEMENTARY NOTES
PAO case number 88ABW-2019-4834, Clearance Date 4 October 2019.Submitted to Optics Express for consideration of publication. The U.S. Government is joint author of this work and has the right to use, modify, reproduce, release, perform, display, or disclose the work. Report contains color.

14. ABSTRACT

We report design and experimental verification of narrowband mid-infrared optical filters with transmission characteristics that are practically constant over a wide range of incident angles. The filter employs a dense array of dielectric resonant cavities in a metal film, and it becomes polarization-independent when geometry of the cavities is azimuthally symmetric.

15. SUBJECT TERMS
filter, photonics

16. SECURITY CLASSIFICATION OF:			17. LIMITATION OF ABSTRACT:	18. NUMBER OF PAGES	19a. NAME OF RESPONSIBLE PERSON (Monitor)
a. REPORT	b. ABSTRACT	c. THIS PAGE			Shivashankar Vangala
Unclassified	Unclassified	Unclassified	SAR	15	19b. TELEPHONE NUMBER *(Include Area Code)* N/A

Angle- and polarization-independent mid-infrared narrowband optical filters using dense arrays of resonant cavities

IVAN AVRUTSKY,[1,*] EVAN M SMITH,[2,3] SHIVASHANKAR VANGALA,[2] RICKY GIBSON,[2,3] JOSHUA R. HENDRICKSON,[2] AND JUSTIN W. CLEARY[2]

[1]*Department of Electrical and Computer Engineering, Wayne State University, Detroit, MI 48202, USA*
[2]*Air Force Research Laboratory, Sensors Directorate, Wright-Patterson AFB, OH 45433, USA*
[3]*KBRwyle Laboratories, Beavercreek, OH 45431, USA*
**ivan.avrutsky@wayne.edu*

Abstract: We report design and experimental verification of narrowband mid-infrared optical filters with transmission characteristics that are practically constant over a wide range of incident angles. The filter employs a dense array of dielectric resonant cavities in a metal film, and it becomes polarization-independent when geometry of the cavities is azimuthally symmetric.

1. Introduction

Applications such as multi-spectral imaging using mosaic-array cameras [1] require polarization-insensitive narrowband spectral filters with transmission characteristics that do not change significantly over a wide range of incident angles. Subject of special interest are filters for the mid-infrared range operating in the atmospheric transparency windows with wavelengths in the 3μm-5μm and 7μm-14μm spectral intervals.

Narrowband filtering can be achieved using Fabry-Perot cavities with multilayer dielectric mirrors. All-dielectric multilayer structures can certainly be scaled to operate in the mid-infrared range [2]. However, Fabry-Perot filters are not angle-independent as the resonant wavelength gets blue-shifted for increased angles of incidence. To some degree the problem can be mitigated by filling the cavity with high-index materials, but the blue shift as such remains an unavoidable feature of the Fabry-Perot resonator with flat mirrors. Another drawback is technological difficulty of depositing multilayers with a rather large total thickness needed for implementing filters operating at longer wavelengths. The latter issue can be addressed by using metal-dielectric [3] instead of all-dielectric multilayers – the metal layers need to be only few dozen nanometer thin. The blue shift of the resonant wavelength remains the issue though.

Another known technique to achieve narrowband filtering is to use guided mode resonances on gratings [4-6]. Periodical thin metal films supporting plasmonic modes also show sharp resonances [7-8]. The filter structure can then be very thin, even in case of a dielectric waveguide-based mid-infrared filter [9], but the spectral resonances are angle-dependent and in many cases polarization-dependent. The physical reason for angular dependence of the resonant wavelength in all of the above cases – from Fabry-Perot resonators excited by oblique incident wave to waveguide gratings to periodical metal films supporting surface modes – is that the resonant field in all these cases is an electromagnetic mode traveling along the lateral direction. Matching the tangential component of the wave vector of the incident wave to the effective wave vector of the traveling mode then sets the link between the incident angle on one side and resonant wavelength on another, and thus the transmission characteristics become angle-dependent.

To break away from the angular dependence of the resonant wavelength, the filter operation should rely upon localized rather than traveling fields. An array of resonators, that are sparse enough to avoid coupling between them, which effectively would lead to formation of a traveling mode that hops from one resonator to the next, and at the same time dense enough to ensure strong resonant transmission, is expected to make an angle-independent filter.

The simplest resonator of this sort, proposed back in 1980 [10], is a narrow slit in a metal film of finite thickness as illustrated in Fig.1 at the left.

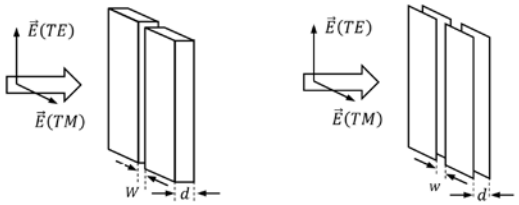

Fig. 1. A narrow slit in a metal film of finite thickness (left), and a pair of thin metal screens with narrow slits (right).

In the direction orthogonal to the plane of the film, light propagates back and forth in a slit as a guided mode in a metal-dielectric-metal waveguide. TM-polarized modes can be supported by infinitely narrow slits, while the slit width W must be at least half-wavelength ($W > \lambda/2$) in size to support TE-modes. Reflections from the edges at the input and output apertures of the slit form Fabry-Perot style transmission resonances when the thickness of the film is close to multiple (m) integer of half-wavelength for the mode in the slit: $d \approx m\lambda/2n^*$, and $n^*$is the modal index for guided modes in the slits. More precise evaluation of the resonant wavelengths should also account for the phase of reflection at the apertures.

At the resonant wavelengths λ_m, assuming the actual width of the slit is small $W \ll \lambda/\pi$, the effective transmission width of the slit for TM-polarized light waves appears to be $W_{eff}^{\perp res} = \lambda_m/\pi$ regardless of the actual slit width. This result was also verified using generic temporal coupled-mode theory in [11]. In a similar manner, effective transmission area in case of a cylindrical cavity terminated by small circular apertures made of perfect metal is $A_{eff}^{res} = (3/4\pi)\lambda^2$ regardless of how small the apertures are [12].

Strikingly, in case of a perfect conductor, even an infinitely narrow slit would resonantly transmit finite amount of optical power $IW_{eff}^{\perp res} = I\lambda_m/\pi$, where I is the intensity of the incident wave. The effective transmission coefficient $W_{eff}^{\perp res}/W$ then diverges at $W \to 0$. Effective transmission width $W_{eff}^{\perp res}$ can also be treated as a width from which light is collected before passing through a much narrower slit. In case of periodical structures with periods comparable or shorter than λ_m/π neighboring resonators will share the area from which they collect incident light and thus be coupled.

Optical filters based on periodical arrays of slits in a metal film have been considered in recent studies [13-16]. These studies often focus on achieving high transmission in the visible spectrum. Slits designed and simulated in one study were determined to achieve angle independence by decoupling the angle-dependent grating resonance from the slit resonance [14]. This was accomplished by reducing the slit width with respect to the periodicity. They also note that mode confinement is enhanced by filling in slits with a high index dielectric medium. Another study fabricated an optical blue filter with polarization insensitivity and angle independence up to 20° using metal disks on a dielectric waveguide [15]. The mode confinement is achieved through a hybridization of surface plasmon modes from the periodicity of the disks and localized Fabry-Perot resonances in the gaps.

Another structure with similar functionality is a pair of thin metal screens with narrow slits [17] as shown in Fig. 1 at the right. Sharp transmission resonances appear when distance between the screens is multiple integer of half-wavelength. Due to possible excitation of

propagating electromagnetic modes in the gap between the conductive planes, the transmission may not be perfect.

Case of TE-polarized waves was recently studied in [18]. For infinitely thin perfectly conducting slotted films the resonant transmission of an optimally focused incident wave reaches unity, even though transmission through a single slit may be infinitely small. This property closely resembles transmission characteristics of a symmetric FP filter with highly reflective mirrors: even with vanishing small transmission through a single mirror, resonant transmission through a pair of mirrors reaches unity. In real metals, the peak transmission drops rather quickly though. For instance, at microwave frequencies in the 10 GHz range the magnitude of the transmission peak for a representative structure, both measured and calculated, was reported to be around 1% [19].

More complicated structures of this sort, with larger number of slotted metal screens, were studied in [20]. Demonstrated filters operate in visible through near infrared spectral range. Additional metal layers help to suppress unwanted transmission peaks and implement a filter with single transmission band in the spectral range of interest.

Reported here are design and experimental verification of narrowband mid-infrared optical filters with transmission characteristics that are practically constant over a wide range of incident angles. We start with a narrow slit configuration as in Fig.1 at the left, with the slits filled with high-index dielectric such as Ge. We proceed to considering slit-like cavities with input/output apertures smaller than the slit width. This helps to better control reflection at the apertures leading to improved filtering characteristics. Then we show that a two-dimensional array of cylindrical cavities with small circular apertures becomes an angle-independent and polarization-independent narrowband filter.

2. Mid-IR nano-resonator filters

2.1 Geometry of the nano-resonators

Possible implementations of Fabry-Perot style filters in a thin metal-dielectric structure are shown in Fig. 2. In the simplest case, this is a dielectric slab cavity terminated by optically thin semitransparent metal films (a). Coupling to/from the resonator involves light transmission through the metal films, which inevitably leads to some optical losses. Using slotted (b) or perforated (e) metal films provides an alternative way of getting light into the resonator – through the voids in the metal films – which may help reducing overall optical losses. Filters of these types will likely show significant angle dependence.

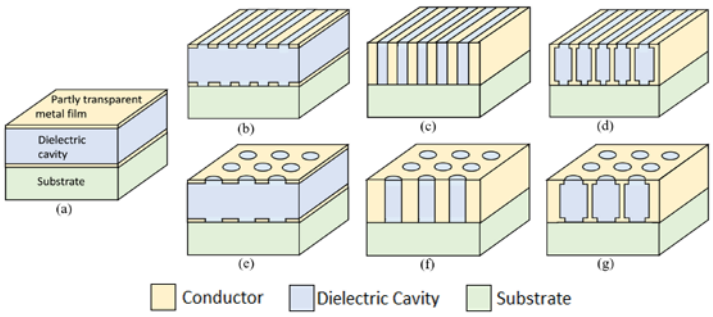

Fig. 2. Variety of implementations of Fabry-Perot style filters

Further sophistication of the filter structure involves breaking the dielectric slab into an array of independent nano-resonators, such as slits (c) or cylindrical holes (f) in an optically thick metal film. With large enough lateral distance between the resonators, the filters or this sort become angle-independent. For better control of light reflection at the input/output apertures of the resonators, the actual apertures with opening smaller than the lateral size of the

resonators can be introduced (d, g). One dimensional arrays (b, c, d) will likely be polarization-dependent, while two-dimensional arrays (e, f, g) can be designed to be polarization-independent.

The structure we start with in this study is a one-dimensional array of nano-resonators (Fig. 2c) with subwavelength apertures (Fig. 2d). The array period is Λ. The structure in general is treated as a three-layer system, with each layer being a slotted metal film. Top and bottom films of thickness t with slit apertures of width w separate the nano-resonators in the middle film from the substrate and cover. The middle film of thickness H has slit-shaped voids with width $W \geq w$ that form the nano-cavities. The resonator dimensions are $H \times W$. The entire structure is held by a substrate assumed to be transparent in the spectral range of interest.

In a particular case, the setting $w = W$ transforms the structure into a single slotted metal film with total thickness of $d = H + 2t$. In this case, it is appropriate to treat the slits as resonators with dimensions $d \times W$. This paper studies angle-independent mid-infrared transmission resonances in a slotted metal film with voids filled with dielectrics with high refractive index n, including the case of actual nano-cavities with $w < W$.

The structure under consideration is schematically shown in Fig. 3. With proper settings for the dimensions and optical constants of the materials, it turns into a narrow slit in a metal film of finite thickness as in Fig. 1 at the left, or into a pair of perforated thin films as in Fig. 1 at the right. Consequently, it is expected that transmission through the narrow apertures will be generally speaking small, except for the wavelengths at which FP-style resonances are excited in the nano-resonators. We find these resonances well suitable for designing angle-independent narrow-band mid-infrared filters. These filters are polarization-dependent though.

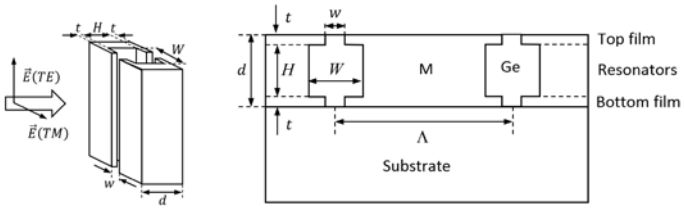

Fig. 3. Details of the nano-resonator array: 3D view (left) and cross section (right).

In simulations below the substrate is a hypothetical lossless dielectric with refractive index of n_s = 1.40, close to that of BaF_2 in the λ = 10μm wavelength range. Barium fluoride is transparent to about 12.5μm while simulation in this paper is continued for slightly longer wavelengths. Material filling the cavities and apertures is a hypothetical lossless dielectric resembling Ge (n = 4.0). Spectral dispersion of both the substrate index and the fillings index at the moment is neglected. The metal (M) permittivity follows Drude formula with plasma frequency $7.25 \cdot 10^4$ cm^{-1} and damping rate $1.45 \cdot 10^2$ cm^{-1}, close to the parameters of Ag. Unless mentioned otherwise, these material parameters are common for all the numerical examples below.

The incident wave, unless mentioned otherwise, is assumed to be TM-polarized.

2.2 Filtering by high-index-dielectric-filled slotted metal films

Representative transmission spectra for slotted metal film ($w = W$, $t = 0$) calculated using the scattering matrix algorithm [20] are shown in Fig. 4. The simulation settings are as follows. The film thickness is d = 1μm, slit width is W = 0.5μm, and the period is Λ = 2μm. Transmission resonances are found for both TE and TM polarized inputs (Fig. 4, left). The TE resonances, as expected, are only visible at shorter wavelengths – the wavelength has to be short enough for TE modes to be guided by the slits. Choice of metal affects the losses in the resonators and thus the maximal transmission at the resonances (Fig. 4, right). Gold and silver show similar

performance, as far as applications in the mid infrared range, while aluminum is significantly worse.

At normal incidence, the transmission spectrum of Ag/Ge structure shows fundamental Fabry-Perot resonance at λ_1 = 8.6μm. Transmission peak reaches 84.5% while transmission between the resonances drops down to about 2.5%. Full width at half maximum for the fundamental transmission resonance is about $\Delta\lambda_1$ = 0.9μm. The resonant wavelength is slightly longer than a simple estimation $2nd$ = 8.0μm based on the index of the material in the slits and thickness of the film. This is partly due to higher modal index n^* for light waves propagating in the slits and partly due to phases of the guided modes reflected at the interfaces with the substrate and cover.

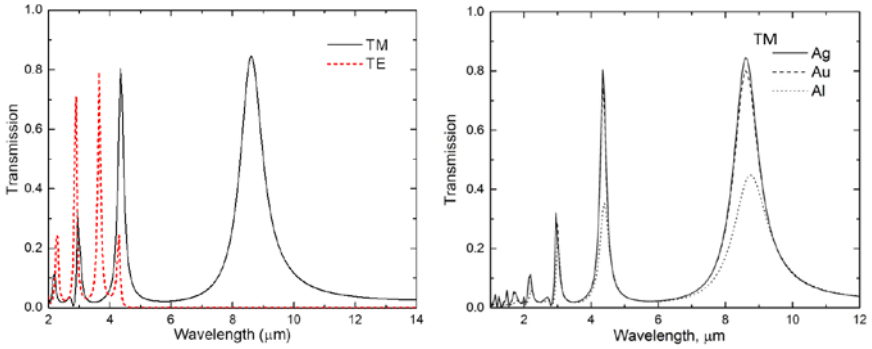

Fig. 4. Representative normal incidence transmission spectra of high-index-dielectric-filled slotted metal films: TM and TE transmission spectra of Ag/Ge structure (left), and TM transmission spectra of Ag/Ge, Au/Ge, and Al/Ge structures.

Second, third, and fourth resonances are at wavelengths close to a half, one third, and one quarter of the fundamental resonance wavelength. As wavelengths of the high-order resonances $\lambda_m \approx \lambda_1/m$, m = 1, 2, 3 … becomes close the structure period Λ = 2.0μm or $n_s\Lambda$ = 2.8μm, the FP-resonances may become coupled with the resonance due to excitation of surface plasmon-polaritons propagating at metal-cover or metal-substrate interface. The latter are angle-dependent and thus fall beyond the scope of interest of this study. Also, at shorter wavelengths assumptions on negligible losses and negligible dispersion of the refractive index in the dielectric fillings no longer match properties of realistic materials.

It is interesting to observe that maximal transmission for the second order resonance is comparable with that for the fundamental resonance, while higher order resonances are much weaker. This correlates well with estimation for the effective transmission width of a single slit. When effective width λ_m/π is getting smaller than the period Λ of the slits, the resonant transmission is roughly estimated at $\lambda_m/\pi\Lambda$ and thus is smaller for resonances at shorter wavelengths, at least in the case of a perfect conductor. The resonances at wavelengths longer than $\pi\Lambda \approx$ 6.3μm are not expected to follow this pattern as effective cross sections of the individual slits overlap.

To further verify the Fabry-Perot nature of the resonances, we traced how the resonant wavelengths change with the film thickness (Fig. 5. left).

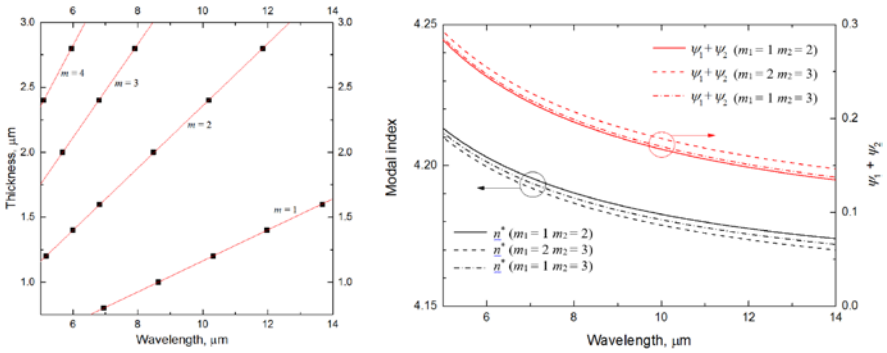

Fig. 5. Resonant wavelengths – film thickness map (left), and modal index and phase change due to reflections at the apertures versus wavelength (right).

Fabry-Perot resonances are observed at wavelengths λ such that the total round trip phase delay is multiple integer of 2π: $2dn^*(\lambda)\cdot 2\pi/\lambda + \psi_1(\lambda) + \psi_2(\lambda) = 2\pi m$, where $\psi_1$and $\psi_2$indicate phase changes associated with guided mode reflections at the top and bottom apertures of the slit. Solving a pair of such equations with resonant orders m_1 and m_2 with respect to $n^*(\lambda)$ and $\psi_1(\lambda) + \psi_2(\lambda)$ allows to find the modal index and combined reflection phase as functions of wavelength (Fig. 5, right). Estimations based on different pairs of resonant orders m_1 and m_2 are rather consistent. As expected for the fundamental TM mode in the slit, the modal index is slightly larger than the index of dielectric in the slit.

Variations of the transmission spectra for the fundamental resonance associated with other than normal incident angles are shown in Fig. 6, left. Transmission spectra for incident angles from 0° to 30° are practically indistinguishable. At larger incident angles the transmission peak is slightly taller and wider, but the resonant wavelength remains the same. In practical sense, the filter retains angle-independent characteristics for incident angles up to about 45°. In relation to applications in imaging devices, *F#* 1.0 corresponds to light cone size of approximately $atan(1/2) \approx 27^o$ as measured with respect optical axis.

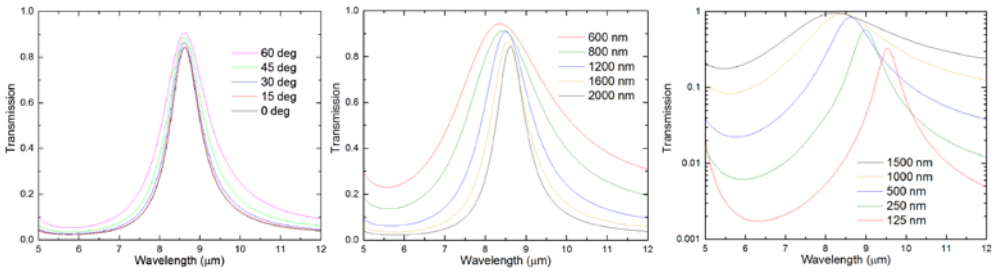

Fig. 6. Main transmission peak for different vales of incident angles (left), structure periods (center), and slit width (right).

For the same reason that resonant wavelengths in the slits are angle-independent, they should not change much with the structure period. Indeed, the angle- and period dependence for transmission resonances on films with gratings is derived from the phase matching condition for excitation of surface modes. In the structures under consideration, each slit is a resonator on its own and periodicity is only an indication of how dense the array of slits is. Thus, it primarily affects the magnitude of the transmission peaks but not the resonant wavelengths. Much longer periods with $\Lambda > \lambda_1/\pi$ will eventually result in substantially reduced peak transmission as effective transmission width becomes smaller than the period.

Resonant transmission peaks for structures with shorter periods are shown in Fig. 6, center. As effective transmission cross sections of individual slits overlap, the resonances in neighboring slits are coupled resulting in wider transmission peaks. Besides broadening the resonance, the coupling leads to formation of a traveling mode that hops from one resonator to another, which eventually entails dependence of the resonant wavelengths on the incident angle.

Effect of slit width variations on the resonant transmission peaks is illustrated in Fig. 6 at the right. As modal index n^* in the narrower gap gets larger, Fabry-Perot resonances in smaller slits are shifted to longer wavelengths. With the slit width decreasing, the resonance becomes sharper, and the suppression of the out-off-band transmission is getting stronger. Peak transmission is lower though. Interestingly, the slit width of 125nm makes only tiny fraction 6.25% of the period while the peak transmission reaches 33% corresponding to effective per-slit transmission coefficient of 5.3. Also notable is that in this case the slit width is only 1.3% of the wavelength. The resonant interactions indeed facilitate rather efficient channeling of electromagnetic energy through the deep subwavelength apertures.

2.3 Filtering by high-index-dielectric-filled nano-cavities

Structures with nano-cavities are formed when top and bottom metal films, as shown schematically in Fig. 3, have apertures with width $w < W$ smaller than width of the cavity W. A representative transmission spectrum for a structure with $H \times W$ = 500nm × 500nm resonators and w = 200nm apertures in t = 50nm resonator terminating films is shown in Fig. 7.

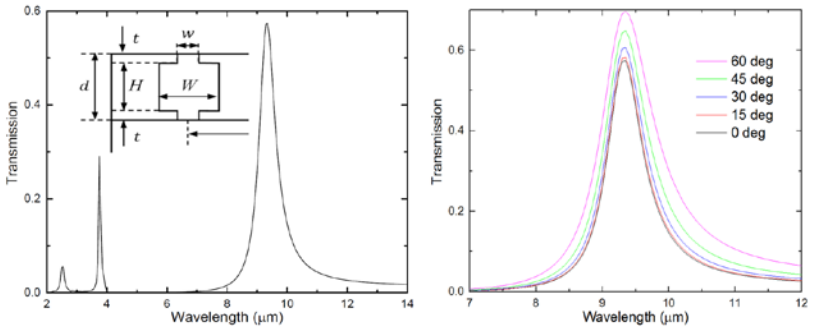

Fig. 7. Transmission resonances of an array of nano-resonators (left) at different incident angles (right). Incident wave is TM-polarized.

Compared to the case of a slit in a film of the same thickness, the fundamental resonant wavelength in the nano-resonator is red-shifted. Resonance is narrower, though maximal transmission is smaller. Free spectral range is wider. Similar to the case of slits, resonant wavelength remains practically the same, peak transmission and spectral width slightly increase with incident angle increasing.

2.4 Filtering by 2D array of high-index-dielectric-filled cylindrical nano-cavities

Filters described above are angle-independent, but not polarization-independent. To achieve polarization-independence, nano-resonators preferably should be axially symmetric. Some polarization dependence may still be present at oblique incidence – even a perfect flat surface shows polarization-dependent reflection and transmission. However, as the resonators as such are isotropic, the filtering characteristics are expected to be largely polarization-independent.

Transmission spectra of two-dimensional arrays of nano-resonators have been simulated using COMSOL (Fig. 8) [22].

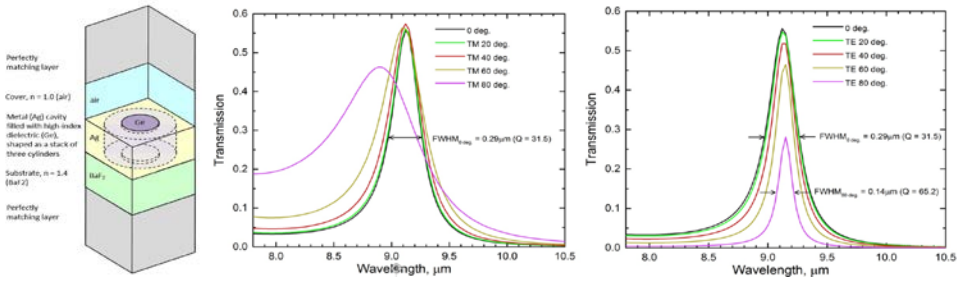

Fig. 8. Cell structure in the simulation (left), and transmission spectra for TM- (center) and TE-polarized (right) input.

The resonators were assumed to be placed in square lattice with period $2\mu m \times 2\mu m$. Each resonant cavity is a cylinder with diameter $1.5\mu m$, height $1.2\mu m$, filled with high-index dielectric (Ge). From the top side the cavity is terminated by a $0.1\mu m$ thick metal film with $1.4\mu m$ coupling aperture filled with the same high-index dielectric. From the substrate side, there is another a $0.1\mu m$ thick metal film with a smaller, $1.15\mu m$, coupling aperture. The substrate, as before, is BaF_2.

Field distribution at the resonant wavelength is shown in Fig. 9. In the horizontal plane in the middle of the resonator, the field is that of the HE_{11} mode of a hollow metal pipe waveguide (turns into TE_{11} mode in case of a perfect conductor). Along the vertical direction, one can recognize the field distribution characteristic to the fundamental mode of a Fabry-Perot resonator, with maximum in the middle and reduced field strength (nodes) at the resonator apertures.

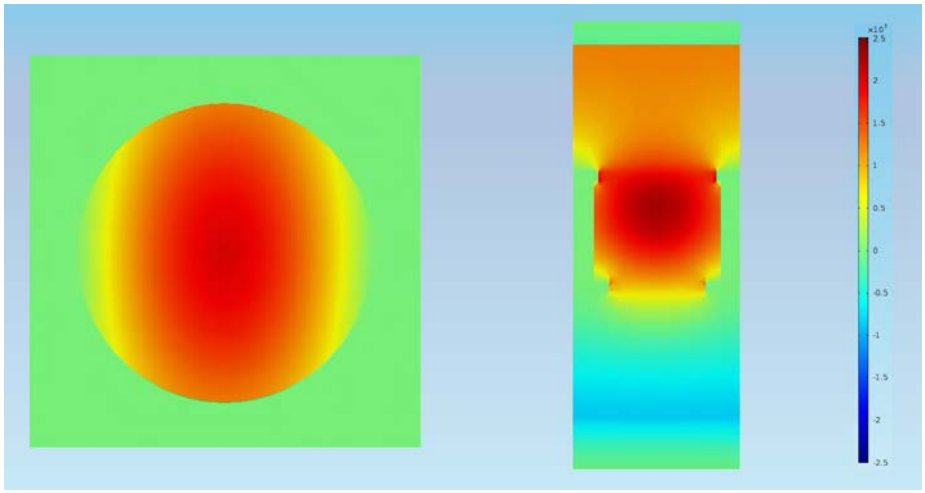

Fig. 9. Resonant electric field strength distribution in a horizontal plane in the middle of the resonator (left) and in the sagittal plane (right).

The resonant transmission is to a great degree both angle- and polarization-independent. To quantify the angle- and polarization dependence of the spectra, we traced the angular dependence of peak wavelength, full width at half maximum, and peak transmission for both polarizations (Fig. 10). In practical sense, significant difference in spectra is found only at the incident angles about 60° and larger.

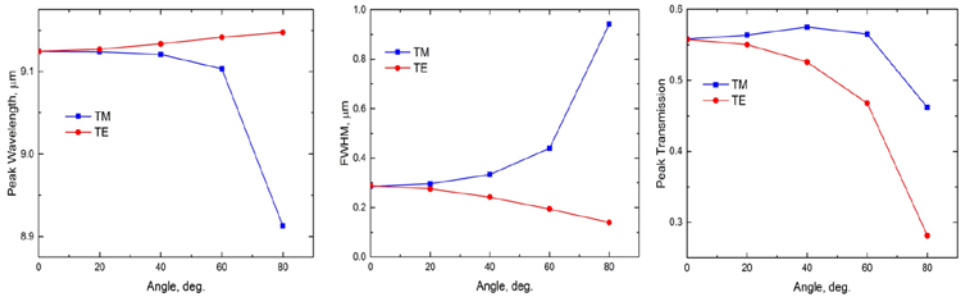

Fig. 10. Peak wavelength (left), full width at half maximum (center), and peak transmission (right) versus the incident angle for both polarizations.

The apertures terminating the resonator cavity help to control the quality factor of the resonance (Fig. 11). Similar to the case of slits, improved quality factor is accompanied by smaller peak transmission – as light wave is kept in the resonator for larger number of round trips, it accumulates more losses due to interaction with imperfectly reflecting metallic walls of the resonator.

The aperture at the substrate side is smaller to symmetrize the reflection coefficients in the Fabry-Perot resonator, which is verified by observing close to zero reflection by the filter structure at the resonance – the incident wave is 100% coupled to the field in the resonators, and then its power is split between the transmission and absorption

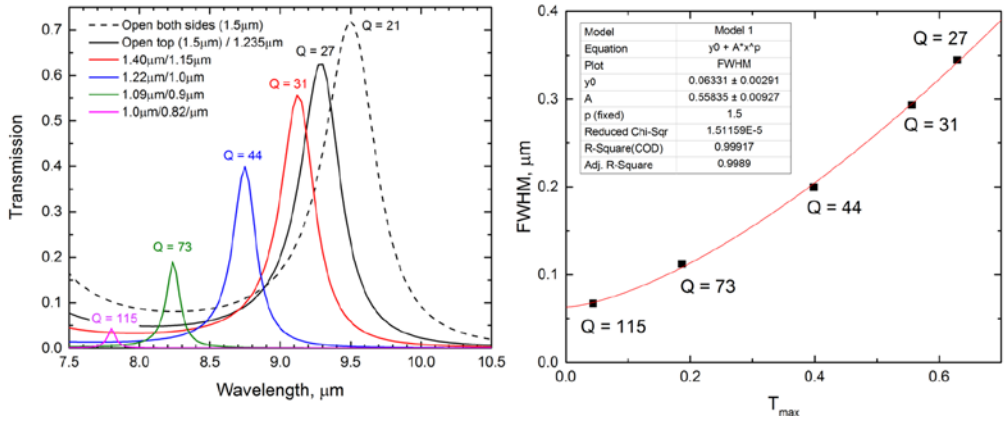

Fig. 11. Resonant transmission peaks for various sizes of the apertures (left), and relation between the full width at half maximum and peak reflection (right).

Smaller coupling apertures result in weaker transmission, but the resonance becomes sharper. Q-factor around 100 is feasible in the LWIR range if $T_{max} \sim 0.1$ is acceptable. The scaling rule appears to be FWHM $\sim T_{max}^{3/2}$. The quality factor in the resonators is limited by absorption in metal walls. Filters based on similar principles are expected to show sharper transmission lines at longer wavelengths in the far infrared and THz spectral range.

3. Experimental verification

Transmission filters were fabricated to match the simulated structures for the simplest case of the one dimensional array design. One advantage of this design is the thin film requirements and the fabrication simplicity – the structure only requires a single patterned layer. The substrate used was barium fluoride. Germanium was first deposited by electron-beam evaporation with a thickness of 1μm. A grating structure with period Λ = 2μm and 0.5μm line width was patterned using contactless stepper photolithography to achieve the small critical

dimensions. Trenches were then etched into the germanium using an anisotropic reactive ion etch process.

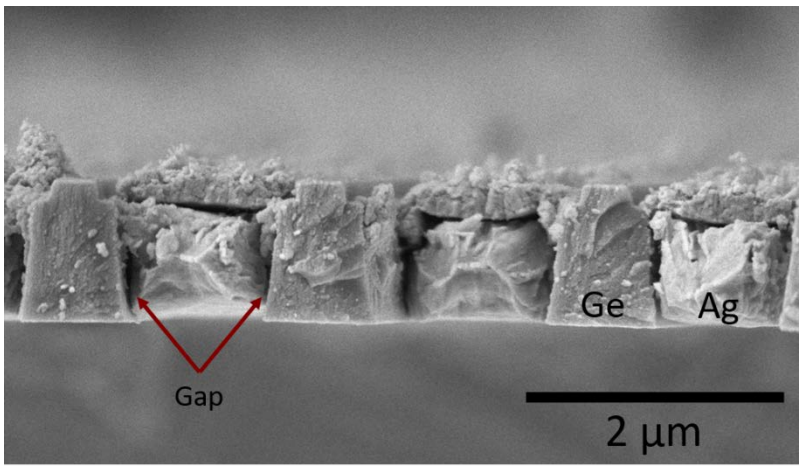

Fig. 12. Cross section of filter structure imaged by scanning electron microscope. Silver is deposited by e-beam evaporation followed by sputtering, resulting in the metal appearing to have two distinct layers. The gaps between the metal and dielectric are on the order of 30-60 nm, although not uniform.

Silver was deposited onto the device prior to the removal of the sacrificial layer used in etching the trenches. Removing the sacrificial layer afterwards leaves Ag in the trenches between the Ge pillars but not on top of them. Upon inspection of a completed device, gaps were observed between the silver and germanium due to shadowing effects from metal depositing on the resist sidewalls, which can be seen in Fig. 12. Various deposition methods were tested in order to mitigate this effect. For the sample shown in Fig. 12, 700 nm silver was deposited by e-beam evaporation, followed by a 300 nm deposition by conformal sputtering. By this method metal partially fills the gaps and reduces their size, while a second layer of metal forms a flat (although rough) top surface. Tilted metal evaporations were also tested, although data is not presented here for those structures.

Transmission spectra for the filters were measured using a Bruker FTIR with a reflecting microscope objective to narrow the incident beam to a small section of the patterned material. Consequently, the incident light on the sample is not parallel but has a light cone of about 12° - 24° which excludes normal incidence. The sample is tilted with respect to normal incidence of this light cone, and for simplicity the sample tilt angles are reported. Transmittance is reported into the BaF_2 substrate; therefore a bare BaF_2 substrate is used as the reference material.

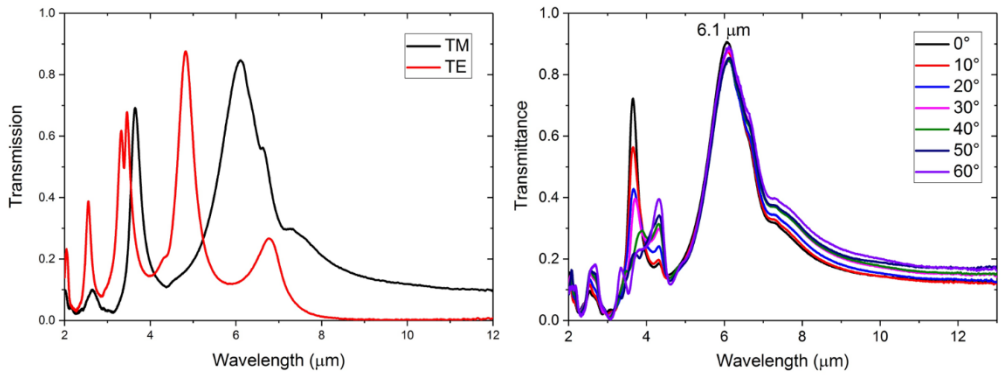

Fig. 13. Experimental transmission spectra for fabricated devices. (Left) Transmission at normal incidence for TM and TE polarizations. (Right) Transmission spectra as a function of angle of incidence for TM-polarized light.

Fig. 13 presents experimental transmission data for both TE and TM polarizations, as well as transmission for various angles of incidence. As predicted by simulations and shown in Fig. 4, different resonant wavelengths are observed for TM and TE polarizations. For each polarization, a fundamental peak is observed with maximum transmission, while lower-order modes are also observed, indicative of a Fabry-Perot resonator and predicted by simulation. For TM polarization, the fundamental resonance is observed at 6.1μm with 84.6% transmission. Transmission drops to 10.8% minimum between the first and second order modes. The full width half maximum for the fundamental mode is $\Delta\lambda_1$ = 1.16μm, slightly wider than the predicted value of 0.9μm. The fundamental transmission peak for TM-polarized light shows little variance as the angle of incidence is increased from 0° up to 60°. The resonant wavelength remains constant at 6.1 μm, while the transmitted intensity varies between 85-90% over the range of angles measured.

While the peak transmission and angular insensitivity match the simulated data, the resonant wavelength deviates significantly from the predicted value of 8.6μm. Additionally, two smaller resonances are observed to be overlapping with the fundamental, one at 6.6μm, which appears as a shoulder on the fundamental peak, and another broad feature centered on 7.3μm, although with only a maximum transmittance of about 30%. The change in resonant wavelength, as well as the additional peaks, are both likely a result of insufficient filling of the gaps between the germanium pillars, as seen in the cross sectional images from Fig. 12. 1-D simulations have shown that small gaps in between the germanium and metal can have a large effect on the resonant wavelength, as shown in Fig. 14. A 10nm rectangular air gap was introduced on both sides of the metal, which shifted the resonant wavelength from 8.6 μm down to 7.3μm. Increasing this gap to 50nm shifts the wavelength down to 5.5μm. When a gap is present, the dielectric chosen to fill the cavity is no longer simply germanium, but rather an effective medium of germanium and air, which has a reduced permittivity. This changes the mode confinement conditions and shifts the resonance. In these cases the peak transmission remains high, the bandwidth narrow and separated from the next harmonic mode.

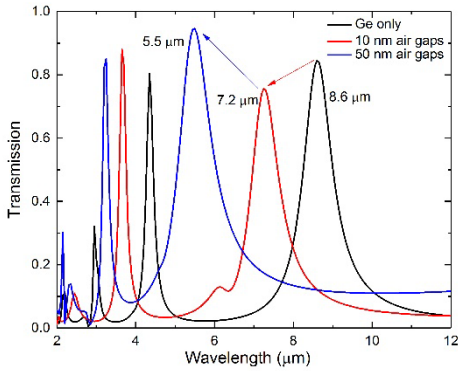

Fig. 14. Simulated transmission spectra for transmission filters at normal incidence for TM-polarized light. The black curve is identical to the transmission from Fig. 4 and represents a cavity completely filled with germanium. The red and blue curves include small gaps in between the metal and dielectric.

The experimental data presented in Fig. 12 represents an averaging over a large area of the fabricated device. Non uniformities across multiple resonators could result in varying air gap sizes, probably between 10-40 nm based on simulations. These non-uniformities create the multiple peaks observed in the experimental data for the fundamental resonant mode. Increasing fabrication uniformity across a large region would eliminate the multiple resonances and decrease the apparent width of the resonant peak. Nevertheless, the experimental results

confirm the predictions provided by the simulations of high transmittance and angular insensitivity up to 60° incidence.

4. Conclusions

In conclusion, we have demonstrated here feasibility of narrowband angle-independent filtering in the mid-infrared spectral range, using arrays of nano-resonators. Experimental data showing high transmittance and angular insensitivity validates the results from simulated structures. Cavities with coupling apertures, compared to slits with straight walls, provide additional degree of freedom tailoring the transmission spectra. Filters based on two-dimensional arrays of axially symmetric cavities, in addition to being angle-independent, are also polarization-independent.

Acknowledgements

We wish to acknowledge support from the Air Force Office of Scientific Research (Program Manager Dr. Gernot Pomrenke) under award number FA9550-19RYCOR048.

References

1. A. V. Kanaev, M. R. Kutteruf, M. K. Yetzbacher, M. J. Deprenger, and K. M. Novak, "Imaging with multi-spectral mosaic-array cameras," Applied Optics **54**(31), F149-F157 (2015).
2. G. Perez, A. M. Bernal-Oliva, E. Marquez, J. M. Gonzalez-Leal, C. Morant, I. Genova, J. F. Trigo, and J. M. Sanz, "Optical and structural characterization of single and multilayer germanium/silicon monoxide systems," Thin Solid Films **485**, 274-283 (2005).
3. C. Sibilia, M. Scalora, M. Bertolotti, M. J. Blomer, and C. M. Bowden, "Electromagnetic properties of periodic and quasi-periodic one-dimensional, metallo-dielectric band gap structures," J. Opt. A: Pure Appl. Opt. **1**, 490-494 (1999).
4. I. A. Avrutsky, G. A. Golubenko, V. A. Sychugov, and A. V. Tishchenko, "Light reflection from the surface of a corrugated waveguide," Soviet Technical Physics Letters **11**, 401-402 (1985).
5. I. A. Avrutsky and V. A. Sychugov, "Reflection of a beam of finite size from a corrugated waveguide," J. Modern Optics **36**, 1527-1539 (1989).
6. R. Magnusson and S. S. Wang, "New principles for optical filters," Appl. Phys. Lett. **61**, 1022-1024 (1992).
7. T. W. Ebbesen, H. J. Lezec, H. F. Ghaemi, T. Thio, and P. A. Wolff, "Extraordinary optical transmission through sub-wavelength hole arrays," Nature **391** (6668), 667-669 (1998).
8. Ivan Avrutsky, Yang Zhao, and Vladimir Kochergin, "Surface-pasmon-assisted resonant tunneling of light through a periodically corrugated thin metal film," Opt. Lett. **9**(25), 595-597 (2000).
9. S. R. Vangala, I. Avrutsky, P. Keiffer, N. Nader, D. Walker, J. W. Cleary, and J. R. Hendrickson, "Asymmetric photonic resonances in GaN slab waveguide for mid infrared selective filters," Opt. Express **22**(20), 24742-24751 (2014).
10. Roger F. Harrington, David T. Auckland, "Electromagnetic transmission through narrow slots in thick conducting screens," IEEE Transactions on Antennas and Propagation **AP-28**(5), 616-622 (1980).
11. Lieven Verslegers, Zongfu Yu, Peter B. Catrysse, and Shanhui Fan, "Temporal coupled-mode theory for resonant apertures," J. Opt. Soc. Am. **B27**(10) 1947-1956 (2010).
12. Yehuda Leviatan, Roger F. Harrington , and Joseph R. Mautz, "Electromagnetic transmission through apertures in a cavity in a thick conductor," IEEE Trans. Antennas and Propagation **AP-30**(6), 1153-1165 (1982).
13. S. Astilean, Ph. Lalanne, M. Palamaru, "Light transmission through metallic channels much smaller than the wavelength," Optics Communications **175**, 265-273 (2000).
14. Jing Zhou and L. Jay Guo, "Achieving angle-insensitive spectrum filter with the slit nanoresonator array structure," J. of Nanophotonics **9**, Art. No. 093795 (2015).
15. Q. Wang, Z. Zhu, H. Gu, Q. Tan, "Angle-tolerant hybrid plasmonic blue filter with polarization-insensitivity and high transmission," Optics Communications **427**, 457-461 (2018).
16. Q. Wang, Z. Zhu, H. Gu, M. Chen, Q. Tan, "Multi-band transmission color filters for multi-color white LEDs based visible light communication," Optics Communications **403**, 330-334 (2017).
17. Yehuda Leviatan, "Electromagnetic coupling between two half-space regions separated by two slot-perforated parallel conducting screens," IEEE Transactions on Microwave Theory and Techniques **36**(1), 44-52 (1988).
18. R. Merlin, "Pinholes meet Fabry-Perot: perfect and imperfect transmission of waves through small apertures," Phys. Rev. **X2**, Art. No. 031015 (2012).
19. S. M. Young, C. Pfeiffer, A. Grbic, and R. Merlin, "Enhanced resonant transmission of electromagnetic radiation through a pair of subwavelength slits," Appl. Phys. Lett. **103**, Art. No. 041104 (2013).
20. Dagny Fleischman, Luke A. Sweatlock, Hirotaka Murakami, and Harry Atwater, "Hyper-selective plasmonic color filters," Optics Express **25**(22), 27386-27395 (2017).

21. M. Liscidini, D. Gerace, L. C. Andreani, J. E. Sipe, “Scattering-matrix analysis of periodically patterned multilayers with asymmetric unit cells and birefringent media,” Phys. Rev. **B77**, Art. No. 035324 (2008).
22. COMSOL Multiphysics® v 5.4. www.comsol.com. COMSOL AB, Stockholm, Sweden.